How to cite: *Angew. Chem. Int. Ed.* **2024**, *63*, e202401626
doi.org/10.1002/anie.202401626

Photoregulation

The Rhodium Analogue of Coenzyme B_{12} as an Anti-Photoregulatory Ligand Inhibiting Bacterial CarH Photoreceptors

Ricardo Pérez-Castaño[+], Juan Aranda[+], Florian J. Widner, Christoph Kieninger, Evelyne Deery, Martin J. Warren, Modesto Orozco, Montserrat Elías-Arnanz, S. Padmanabhan,* and Bernhard Kräutler**

Dedicated to the memory of Albert Eschenmoser

Abstract: Coenzyme B_{12} (AdoCbl; 5′-deoxy-5′-adenosylcobalamin), the quintessential biological organometallic radical catalyst, has a formerly unanticipated, yet extensive, role in photoregulation in bacteria. The light-responsive cobalt-corrin AdoCbl performs this nonenzymatic role by facilitating the assembly of CarH photoreceptors into DNA-binding tetramers in the dark, suppressing gene expression. Conversely, exposure to light triggers the decomposition of this AdoCbl-bound complex by a still elusive photochemical mechanism, activating gene expression. Here, we have examined AdoRhbl, the non-natural rhodium analogue of AdoCbl, as a photostable isostructural surrogate for AdoCbl. We show that AdoRhbl closely emulates AdoCbl in its uptake by bacterial cells and structural functionality as a regulatory ligand for CarH tetramerization, DNA binding, and repressor activity. Remarkably, we find AdoRhbl is photostable even when bound "base-off/His-on" to CarH in vitro and in vivo. Thus, AdoRhbl, an antivitamin B_{12}, also represents an unprecedented anti-photoregulatory ligand, opening a pathway to precisely target biomimetic inhibition of AdoCbl-based photoregulation, with new possibilities for selective antibacterial applications. Computational biomolecular analysis of AdoRhbl binding to CarH yields detailed structural insights into this complex, which suggest that the adenosyl group of photoexcited AdoCbl bound to CarH may specifically undergo a concerted non-radical *syn*-1,2-elimination mechanism, an aspect not previously considered for this photoreceptor.

Introduction

The organometallic cobalt-corrin coenzyme B_{12} (AdoCbl; 5′-deoxy-5′-adenosylcobalamin)[1] (Figure 1) is an intriguing enzyme cofactor[2] thanks to its remarkable ability to serve as a reversibly functioning source of an Ado radical.[3] AdoCbl is also a highly light-sensitive source for the Ado radical, which is photogenerated in solution from AdoCbl on a picosecond time scale.[4] However, no physiological function for this fundamental property of AdoCbl, its photosensitivity, was envisioned. Unexpectedly, nature has indeed exploited this inherent characteristic of AdoCbl. It is

[*] R. Pérez-Castaño,[+] Prof. Dr. M. Elías-Arnanz
Departamento de Genética y Microbiología, Área de Genética (Unidad Asociada al IQFR-CSIC), Facultad de Biología
Universidad de Murcia
30100 Murcia (Spain)
E-mail: melias@um.es

Dr. J. Aranda,[+] Prof. Dr. M. Orozco
Institute for Research in Biomedicine (IRB Barcelona)
Baldiri Reixac 10–12, 08028 Barcelona (Spain)

Dr. F. J. Widner, Dr. C. Kieninger, Prof. Dr. B. Kräutler
Institute of Organic Chemistry & Center for Molecular Biosciences
University of Innsbruck
Innrain 80/82, A-6020 Innsbruck (Austria)
E-mail: bernhard.kraeutler@uibk.ac.at

Dr. E. Deery, Prof. Dr. M. J. Warren
School of Biosciences
University of Kent
Canterbury, CT2 7NJ (UK)

Prof. Dr. M. J. Warren
Quadram Institute Bioscience, Norwich Research Park, Norwich NR4 7UQ, UK

Prof. Dr. M. Orozco
Institute for Research in Biomedicine (IRB Barcelona), The Barcelona Institute of Science and Technology, Barcelona (Spain); the Joint BSC-IRB Research Program in Computational Biology, and Department of Biochemistry and Biomedicine, University of Barcelona
Baldiri Reixac 10–12, 08028 Barcelona (Spain)

Prof. Dr. S. Padmanabhan
Instituto de Química Física Blas Cabrera (IQF-CSIC)
Consejo Superior de Investigaciones Científicas (CSIC)
119 c/Serrano, 28006, Madrid (Spain)
E-mail: padhu@iqf.csic.es

[+] Contributed equally

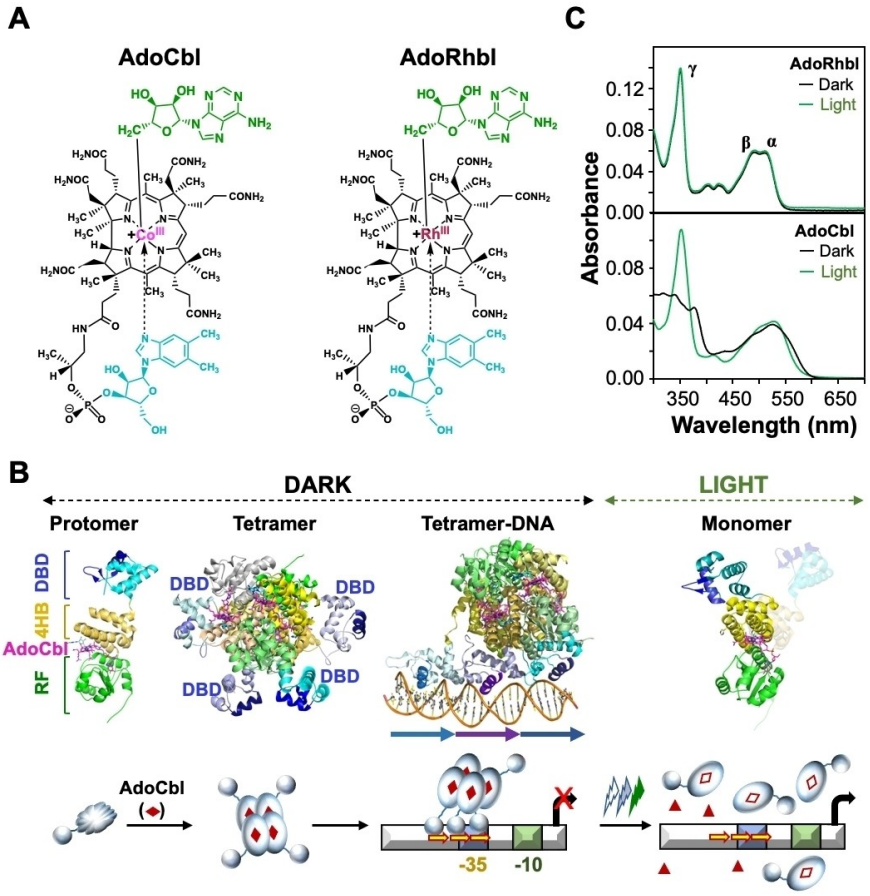

Figure 1. Coenzyme B_{12} (AdoCbl), its rhodium homolog AdoRhbl, and CarH photoreceptor structures and mechanism of action. (**A**) Structural formulae of base-on AdoCbl (left) and AdoRhbl (right). (**B**) Top: Structures of the AdoCbl-$CarH_{Tt}$ protomer, the free and DNA-bound tetramer, and the light-exposed monomer (PDB codes, 5C8D, 5C8E and 5C8F, respectively). DNA-binding domain (DBD) is in cyan, with recognition helix and wing in dark blue; in the AdoCbl-binding module with bound AdoCbl (magenta), the four-helix bundle (4HB) is in golden and the Rossmann fold (RF) in green. Arrows below the DNA-bound structure indicate the three 11-bp direct repeats of the $CarH_{Tt}$ operator. Bottom: Schematic of the $CarH_{Tt}$ mode of action. AdoCbl (red diamond) binding to apo form CarH monomer produces AdoCbl-bound tetramers that bind to operator DNA (overlapping the promoter) to repress transcription. Light disrupts tetramers to monomers via AdoCbl photolysis (photolyzed cobalamin: empty diamonds; released photolysis product: red triangles) to abolish operator binding and activate transcription. (**C**) UV/Visible spectra of aqueous solutions of AdoRhbl (top; α, β, γ bands indicated) and AdoCbl (bottom) in the dark and after exposure to white light.

utilized as a light-sensing chromophore within the widespread family of bacterial CarH photoreceptors,[5] thus revealing a fundamental, nonenzymatic biological role of AdoCbl in photoregulation.[5] Further investigations uncovered B_{12}-based photoregulation in AerR proteins within photosynthetic bacteria,[6] and genome analyses have identified numerous uncharacterized proteins with CarH-like AdoCbl-binding light sensor modules, either as stand-alone entities or fused to other functional domains.[5b–d,6–7]

In AdoCbl, a Co^{III} center carries a 5′-deoxyadenosyl group (Ado) as the 'upper' ligand, while a 5,6-dimethylbenzimidazole (DMB) nucleotide extends from the corrin core beneath the molecule, coordinating to the 'lower' axial position of Co^{III} in the stable 'base-on' form (Figure 1).[1a] CarH photoreceptors, however, bind their AdoCbl ligand in the alternative 'base-off/His-on' form, where the Co-coordinated lower axial DMB ligand is replaced by a protein histidine.[8] These photoreceptors respond to UV, blue and green light, modulating CarH oligomerization, DNA binding and light-induced disruption,[5] showcasing unique properties that have inspired exciting applications in optogenetics, synthetic biology, smart materials, and catalysis.[5c,d,9]

CarH homologs from *Thermus thermophilus* ($CarH_{Tt}$), *Bacillus megaterium* ($CarH_{Bm}$), and *Myxococcus xanthus* ($CarH_{Mx}$) have been extensively characterized in vitro and/or in vivo.[5,8,10] In particular, crystal structures of $CarH_{Tt}$ in its free, DNA-bound, and light-exposed forms,[8,10a] together with detailed studies of its oligomerization,[5a,8,10a,c,h] and unprecedented photochemistry[10a,d–g,m,n] are available. These have established that: (a) AdoCbl binds specifically to $CarH_{Tt}$ in a base-off/His-on form, and the upper axial Ado group is clearly reoriented, compared to free AdoCbl;[5a,8,10a,11] (b) AdoCbl binding drives $CarH_{Tt}$ oligomerization, DNA binding and transcriptional repressor activity in the dark; (c) light cleaves the Co–C bond of the bound AdoCbl, inducing a large protein structural shift that disrupts the $CarH_{Tt}$ tetramer and its operator binding to allow transcription (Figure 1B).[5a,b,8,9h,10a,c,h] Interestingly,

$CarH_{Tt}$ plays a crucial role in the secure utilization of AdoCbl in light-dependent gene regulation by releasing the non-radical product, 4′,5′-anhydroadenosine, instead of the highly reactive Ado radical.[10d] The precise process through which $CarH_{Tt}$ accomplishes this task remains elusive, despite considerable efforts dedicated to understanding the underlying photochemical mechanism.[10a,d–g,m,n] These properties observed with $CarH_{Tt}$ are conserved in vivo by $CarH_{Mx}$,[5a,b,10b,l] and in vitro and in vivo by $CarH_{Bm}$, albeit with variations suggesting plasticity within otherwise conserved modes of AdoCbl binding, oligomerization, and DNA binding (compare models in Figure 1B and S1).[10i,j]

Here, we describe the first study of CarH function in vitro and in vivo using 5′-deoxy-5′-adenosylrhodibalamin (AdoRhbl), the non-natural, light-stable, structural mimic of AdoCbl, in which the essential Co^{III}-center of AdoCbl is replaced by a Rh^{III} ion (Figure 1A).[12] Our objective was to uncover whether and how AdoRhbl binds to CarH and affects its light-dependent oligomerization, DNA binding and photoregulatory function. Additionally, we sought to investigate whether CarH alters AdoRhbl photochemistry, akin to its interactions with AdoCbl. Crystal structures of AdoRhbl[12a,b] and of various other B_{12} analogues featuring alternative metals in place of the natural cobalt-center[1,2c,d,13,14] have been recently reported. These analogues serve as antivitamins B_{12}, proving useful for biological and biomedical studies.[14c,15] Notably, AdoRhbl inhibits the growth of *Salmonella enterica* and acts as a potent inhibitor of propanediol-dehydratase,[12a] an enzyme reliant upon AdoCbl bound base-on.[16] However, the binding interactions of AdoRhbl with AdoCbl-dependent proteins has not yet been reported. Significantly, unlike the photosensitive AdoCbl with its characteristic "atypical" UV/Vis-spectrum,[4a,b,17] AdoRhbl displays a "typical" corrin spectrum (Figure 1C) and is photostable.[12a] As reported here, AdoRhbl closely mimics AdoCbl in adopting a 'base-off/His-on' mode of binding to CarH, and in inducing CarH tetramerization and DNA binding. Nevertheless, AdoRhbl is observed to remain photoinactive even when in complex with CarH. Thus, AdoRhbl acts as an unprecedented anti-photoregulatory ligand. Our computational analysis indicates that the structural integrity of AdoRhbl-bound CarH is largely unperturbed relative to the natural AdoCbl-bound form but allows the Ado moiety of the AdoRhbl to adopt more conformational forms within the binding pocket. These findings offer initial structural insights likely relevant to the ongoing debate on the puzzling non-radical mechanism[10n] underlying CarH-directed AdoCbl photochemistry.

Results and Discussion

We first assessed if AdoRhbl binds to $CarH_{Tt}$ (the most extensively characterized CarH homolog), induces $CarH_{Tt}$ tetramerization in the dark, and responds to light, using size-exclusion chromatography (SEC). The apo form of $CarH_{Tt}$ elutes as a monomer with an apparent molecular mass of 36 kDa, comparable to 33.1 kDa, estimated from sequence or by mass spectrometry, but elutes as a tetramer (~140 kDa) in the dark or in the light in the presence of AdoRhbl, with the latter bound as indicated by the absorbance at 522 and 280 nm of the eluted peak (Figure 2A). Thus, like AdoCbl, AdoRhbl binds to $CarH_{Tt}$ and drives its tetramer formation. However, light disrupts the AdoCbl-$CarH_{Tt}$ tetramers to monomers, but not the AdoRhbl-$CarH_{Tt}$ tetramers. We next tested the effects of AdoRhbl on the homolog $CarH_{Bm}$, which varies from $CarH_{Tt}$ in the mode of oligomerization and DNA binding.[10i,j] Previous studies showed that in the absence of AdoCbl, $CarH_{Bm}$ elutes as non-DNA binding oligomers (established spectroscopically to have a loosely folded molten globule structure), distinct from the AdoCbl-bound tetramers that bind tightly and specifically to DNA in the dark; and that light disrupted these to yield photolyzed, non-DNA binding dimers (Figure S1).[10j] Here, we find that AdoRhbl binds to apo$CarH_{Bm}$ (109 kDa; calculated mono-

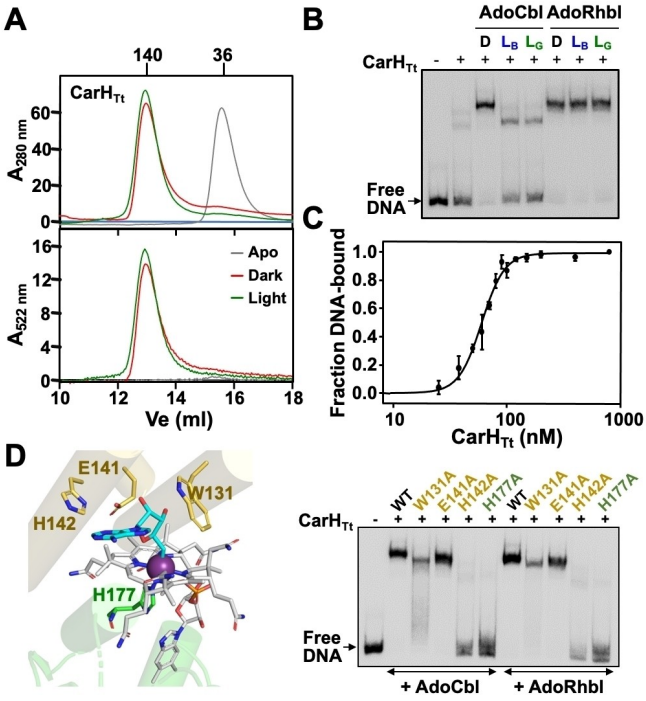

Figure 2. Effect of AdoRhbl on $CarH_{Tt}$ oligomerization and DNA binding. (**A**) SEC profiles (Superdex200 analytical column) of $CarH_{Tt}$ in the apo form and with AdoRhbl in the dark or after 5-min exposure to green light (apparent molecular mass in kDa indicated on top). (**B**) Representative EMSA for $CarH_{Tt}$ binding to a 130-bp operator DNA probe without and with 5-fold molar excess of AdoCbl or AdoRhbl in the dark ("D") or after 5-min exposure to blue ("L_B") or green ("L_G") light. Uncropped gel is shown in Figure S14A. (**C**) Estimates of the $CarH_{Tt}$ DNA binding affinity (K_D) and Hill coefficient *n* from fits of EMSA data in the presence of AdoRhbl (Figure S3) to the Hill equation. (**D**) Left: Close-up of the dark $CarH_{Tt}$ tetramer AdoCbl-binding pocket (PDB ID 5C8D) highlighting Trp131, Glu141, and His142 (gold) of the Wx_9EH motif capping the Ado group (cyan) of AdoCbl (gray with cobalt as magenta sphere), and the lower axial cobalt ligand His177 (green). Right: EMSA binding of the indicated $CarH_{Tt}$ mutants to the 130-bp DNA probe in the dark with 5-fold molar excess of AdoCbl or AdoRhbl. Uncropped gel is shown in Figure S14B.

mer molecular mass 36.3 kDa) and induces formation of tetramers (156 kDa) that persist when exposed to light (Figure S2), in marked contrast to the light-induced dissociation of AdoCbl-CarH$_{Bm}$ tetramers to dimers.[10j]

AdoCbl-bound CarH tetramers bind specifically to DNA in the dark and this is abolished by light (Figures 1B and S1). In vitro, this can be readily monitored using electrophoretic mobility shift assays (EMSA). In the dark, using a specific 130-bp DNA probe containing the CarH$_{Tt}$-binding site, EMSA revealed a well-defined retarded band for the CarH$_{Tt}$-DNA complex formed in the presence of AdoRhbl, as observed for AdoCbl, but the band with AdoRhbl present (unlike with AdoCbl) persisted after exposure to blue or green light (Figure 2B). The apparent CarH$_{Tt}$-DNA binding affinity, K_D, estimated from EMSA data with AdoRhbl present was (60 ± 2) nM, with a Hill coefficient of (4.3 ± 0.4) consistent with cooperative tetramer binding (Figures 2C and S3), quantitatively matching the observations with AdoCbl.[8] Analogous results were obtained for the binding of CarH$_{Bm}$ to its specific DNA probe with AdoRhbl versus AdoCbl (Figure S4A). Thus, like AdoCbl, AdoRhbl not only enables CarH tetramerization but also its specific binding to DNA in vitro and yet, in contrast to AdoCbl, the DNA-bound complex with AdoRhbl is insensitive to light.

Crystal structures of CarH$_{Tt}$ revealed AdoCbl sandwiched between a four-helix bundle containing a highly conserved Wx$_9$EH motif surrounding the upper axial Ado and a Rossman fold subdomain (Figure 1B and 2D). Furthermore, the His of the canonical ExHx$_2$G/Px$_{41}$SxTx$_{22-27}$GG B$_{12}$-binding motif in CarH displaces DMB as the lower axial Co^{3+} ligand in a base-off/His-on mode of binding.[8] Single mutations of conserved residues in the two motifs impair or abolish formation of active tetramer repressors and thereby DNA binding.[5a,8,10j] We therefore tested using EMSA how purified CarH bearing each mutation binds to DNA in the presence of AdoRhbl versus AdoCbl. Variants with single mutations to Ala of Trp, Glu or His of the Wx$_9$EH motif, and of the His required for B$_{12}$ base-off/His-on binding were tested (Figures 2D and S4B). DNA binding in the dark by each CarH$_{Tt}$ mutant, with AdoRhbl present, matched that with AdoCbl: little or no DNA binding by the two His mutants, weak binding by the Trp mutant, and marginally affected binding by the Glu mutant (Figure 2D). Similar results were obtained with AdoRhbl versus AdoCbl for equivalent CarH$_{Bm}$ variants:[10j] poor or no DNA binding for the Trp, Glu and the lower axial His mutants; weak binding for the upper His mutant (Figure S4B). The data are thus consistent with AdoCbl-like base-off/His-on binding of AdoRhbl to CarH photoreceptors. Mutating two Gly to the larger Gln at the CarH$_{Tt}$ dimer-dimer interface impairs tetramer formation and yields dimers, instead.[8] For both these CarH$_{Tt}$ Gly mutants, DNA-binding with AdoRhbl resembled that with AdoCbl: a lower (faster mobility) band for the dimer and an upper band with mobility similar to the single wild-type CarH$_{Tt}$ tetramer band that would correspond to the binding of two Gly mutant dimers to the DNA site (Figure S5). Thus, these data indicate that the CarH mode of ligand-binding, tetramerization and DNA binding appear to be very similar in the presence of AdoRhbl or AdoCbl.

The αβ band of the AdoCbl UV/Visible spectrum redshifts upon titration with CarH$_{Tt}$ (Figure S6), which enabled an estimate of its binding affinity (K_D) to AdoCbl as ~250 nM (~210 nM for CarH$_{Bm}$).[10e,j] The AdoRhbl αβ band also redshifts upon titration with CarH$_{Tt}$, from which a K_D of around 6 μM was obtained (see Figure 3), reflecting a roughly 25-fold weaker CarH binding to AdoRhbl than to AdoCbl. In the in vitro tetramerization and DNA binding assays above (Figure 2), excess AdoCbl or AdoRhbl may have masked the lower affinity of CarH$_{Tt}$ for AdoRhbl.

Next, we investigated how the in vitro binding of AdoRhbl, which induces both CarH tetramerization and binding to DNA without any response to light, translates into in vivo effects (Figure 4). Light and B$_{12}$-dependent CarH oligomerization can be readily assessed in vivo using a bacterial two-hybrid (BACTH) system in *Escherichia coli*, which does not synthesize corrinoids but can acquire them from its growth medium.[5a] In this assay, based on the interaction-mediated reconstitution of adenylate cyclase enzymatic activity in *E. coli*, a blue color on X-Gal plates indicates physical interaction between the proteins tested (see Experimental Procedures in the Supporting Information for details). Accordingly, cells expressing two-hybrid fusions of CarH$_{Mx}$ or CarH$_{Tt}$ self-interact only in the dark and with AdoCbl present, whereas cells expressing fusions to a B$_{12}$-independent CarH$_{Mx}$ paralog, CarA$_{Mx}$, self-interact in the dark or in the light with or without AdoCbl present, and serve as a positive control (Figure 4A). Compared to cells grown with AdoCbl, those grown with AdoRhbl acquired a lighter blue color in the dark that persisted in the

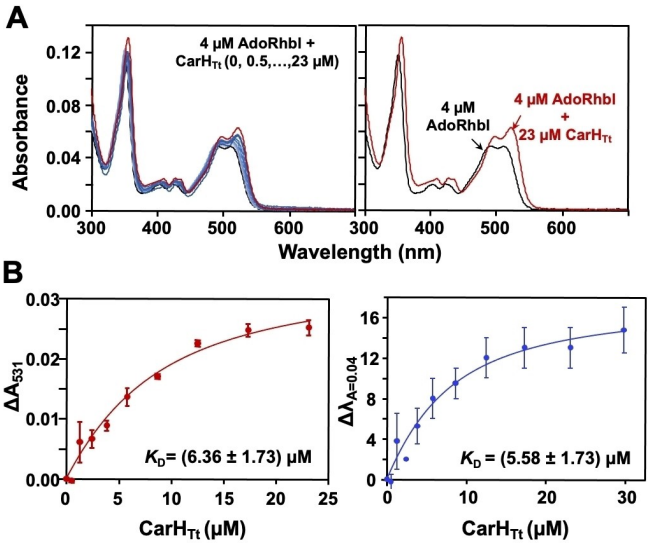

Figure 3. Spectral evolution of AdoRhbl titrated with CarH$_{Tt}$ and determination of binding affinity. (**A**) UV/Visible spectra of AdoRhbl (4 μM fixed concentration) titrated with 0 to 23 μM CarH$_{Tt}$ (left), and traces for the first and last titration points (right). (**B**) CarH$_{Tt}$-AdoRhbl binding affinity (K_D) estimated from titrations as in **(A)** by fitting absorbance change at 531 nm, ΔA_{531} (left) or wavelength shift at fixed intensity, $\Delta\lambda_{0.04}$ (right).

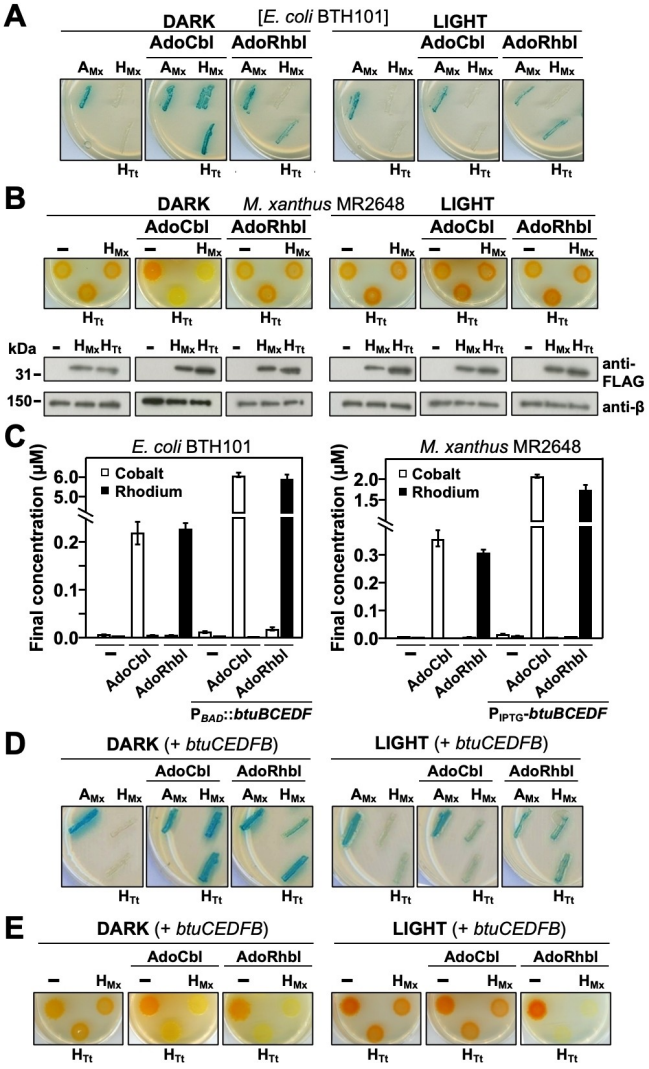

Figure 4. Effect of AdoRhbl on CarH oligomerization and function in vivo. (**A**) Two-hybrid analysis in *E. coli* BTH101 cells expressing T25 and T18 fusions of $CarH_{Mx}$ ("H_{Mx}"), $CarH_{Tt}$ ("H_{Tt}") or, as positive control under all tested conditions, $CarA_{Mx}$ ("A_{Mx}"). Streaks of cells on LB-Kan-Amp agar plates containing X-Gal and IPTG without or with AdoCbl or AdoRhbl grown in the dark or in white light. Blue streak indicates self-interaction. (**B**) Color phenotype of *M. xanthus* strains MR2648 (recipient, negative control, "-"), and MR2998 ("H_{Mx}") or MR2903 ("H_{Tt}"), with vanillate-inducible expression of FLAG-tagged $CarH_{Mx}$ and CTt2, respectively, grown on CTT-agar-vanillate plates, without or with AdoCbl or AdoRhbl in the dark or in white light. Below: western blots of cell extracts using anti-FLAG (top), or anti-RNA polymerase β subunit antibodies as loading control (bottom). Uncropped blots are shown in Figure S15. (**C**) ICP-MS analysis of intracellular cobalt (unfilled bars) and rhodium (black bars). Left: *E. coli* BTH101 grown in LB, or LB-Spt-arabinose medium with B_{12} transporter proteins overexpressed from plasmid pBAD42-*btuCEDFB*, without and with AdoCbl or AdoRhbl. Right: *M. xanthus* MR2648 grown in CTT, or in CTT-Tet medium with 1 mM IPTG-induced *btuCEDFB* expression, without and with AdoCbl or AdoRhbl. (**D**) Two-hybrid analysis (as in **A**) with pBAD42-*btuCEDFB* expressed and streaked on LB-Kan-Amp-Spt agar plates with X-Gal, IPTG, and arabinose, without and with AdoCbl or AdoRhbl, and grown in the dark or light. (**E**) Color phenotype of *M. xanthus* strains MR3694 (negative control, "−"), MR3695 ("H_{Mx}") and MR3696 ("H_{Tt}"), with vanillate-induced expression of N-terminal FLAG-tagged $CarH_{Mx}$ and CTt2, respectively, and grown on CTT-agar plates with IPTG and without and with AdoCbl or AdoRhbl in the dark or light.

light when two-hybrid fusions of $CarH_{Tt}$ were expressed, while a blue color was not seen when $CarH_{Mx}$ fusions were expressed (Figure 4A). Thus, AdoRhbl is not as effective as AdoCbl in driving CarH self-interaction in vivo, and any induced CarH tetramerization is not abrogated by light.

To assess the impact of AdoRhbl on the light-dependent CarH repressor function in vivo, experiments were conducted using the *M. xanthus* strain MR2648, which lacks the native genes for $CarH_{Mx}$, $CarA_{Mx}$ and PduO (Table S1). Elimination of the PduO adenosyltransferase that generates AdoCbl, enables control of intracellular AdoCbl.[10j] Wild-type *M. xanthus* is yellow in the dark but becomes orange red in the light due to carotenoid pigments. In MR2648, genes for carotenoid biosynthesis are derepressed because CarH and CarA are absent, and these cells are therefore orange under both dark and light conditions (Figure 4B).[10j]

By conditionally expressing the CarH variants in the MR2648 genetic background, it becomes possible to explore their repressor activity in vivo. Only a functional CarH can restore the yellow colony color in the dark when AdoCbl is present. Consequently, in the MR2648 strain, we proceeded to conditionally express $CarH_{Mx}$ or the $CarH_{Tt}$ surrogate CTt2,[5a] both tagged with an N-terminal FLAG epitope to verify their stable expression using western blots (Figure 4B). CTt2 is an established variant comprising the fusion of $CarH_{Mx}$'s C-terminal DNA-binding domain with $CarH_{Tt}$'s N-terminal AdoCbl-binding domain.[5a] With AdoCbl present, MR2648 expressing $CarH_{Mx}$ or CTt2 was yellow in the dark, consistent with repression of carotenoid synthesis, and turned orange red in the light due to derepression. By contrast, the cells remained orange red in the dark or in the light with AdoRhbl present despite stable expression of $CarH_{Mx}$ and CTt2 as verified in western blots (Figure 4B), indicating negligible repressor activity. Thus, CarH repressor activity in *M. xanthus*, observed with AdoCbl, was barely detectable with AdoRhbl.

As the observed reduction in the in vivo CarH activity with AdoRhbl may result from insufficient cellular uptake, we compared the uptake of AdoRhbl and AdoCbl in *E. coli* and *M. xanthus* strains. Each strain was grown in media in the presence or absence of 1 μg/ml (~0.6 μM) AdoCbl or AdoRhbl under identical conditions, and the cells were harvested and analyzed. As acid-sensitivity of the organometallic bonds of AdoCbl[18] and AdoRhbl made an LC-MS/MS approach for estimating cellular AdoCbl contents[19] unsuitable under our conditions, we employed ICP-MS as a method to simultaneously measure Co and Rh. ICP-MS detected negligible Co or Rh in *E. coli* BTH101 or *M. xanthus* MR2648 cells grown without exogenous AdoCbl or AdoRhbl and detected Co but no Rh in cells grown with exogenous AdoCbl and, at a similar level, Rh but no Co in cells grown with exogenous AdoRhbl (Figure 4C and Figure S7). Our data thus indicate ICP-MS as a valid approach to determine intracellular levels of AdoCbl or AdoRhbl.

Co and Rh contents determined by ICP-MS in *M. xanthus* MR2648 yielded an approximate intracellular concentration of (4.9 ± 0.1) μM for AdoCbl and (4.5 ± 0.2) μM for AdoRhbl, reasonably close to the independently estimated total intracellular cobalamin (3.8 ± 0.5 μM) (Ta-

ble S2). The intracellular AdoRhbl concentration in *M. xanthus* is, thus, comparable to the K_D (~6 μM) determined for $CarH_T$-AdoRhbl binding in vitro that, combined with competition from other B_{12}-binding proteins, may render AdoRhbl levels insufficient for detectable CarH binding, tetramerization, and function in vivo. Limited AdoRhbl content also likely accounts for the results of two-hybrid analysis in *E. coli* (Figure 4A), in which ICP-MS detected Co and Rh at levels comparable to those in *M. xanthus* (Figures 4C and S7B). This could conceivably be offset by augmenting intracellular AdoRhbl levels, as was tested next.

Bacterial uptake of exogenous B_{12} is controlled tightly by mechanisms such as those involving RNA-based B_{12} riboswitches, which typically downregulate genes encoding proteins for cobalamin biosynthesis and transport.[13b,20] These riboswitch controls have been bypassed to enhance intracellular cobalamin levels in *E. coli* by overexpressing its genes for B_{12} transport and utilization (*btu*), including *btuC*, *btuE*, *btuD*, *btuF*, and *btuB* (hereafter, *btuCEDFB*) from an arabinose-inducible P_{BAD} promoter (Figure S7A).[19] Using ICP-MS, we determined that arabinose-induced overexpression of *btuCEDFB* in *E. coli* strains used in two-hybrid analysis (BTH101) and in protein overexpression (BL21-DE3) increased Co concentration ~25–30 fold in cells grown with AdoCbl present relative to cells grown under identical conditions, but without *btuCEDFB* overexpressed (Figures 4C and S7). Interestingly, growing these *E. coli* strains with AdoRhbl present produced similar enhancements in intracellular Rh levels. Moreover, overexpressing the same *E. coli btuCDEFB* genes from an IPTG-inducible promoter in *M. xanthus* strain MR2648 grown in the presence of AdoCbl or AdoRhbl enhanced intracellular Co or Rh levels nearly six-fold (Figure 4C).

The observed similar enhancement of the intracellular accumulation of AdoRhbl and AdoCbl upon overexpression of *btuCEDFB* in *E. coli* or in *M. xanthus* indicates that these transporter proteins bind and transport AdoRhbl in a very similar fashion to AdoCbl. This accords with the ability of these transporters to bind to diverse B_{12} forms base-on and with high affinities.[21] In BACTH analysis using *E. coli* BTH101 with this enhanced intracellular AdoRhbl, self-interaction in the dark, which persisted in the light, was now detected for $CarH_{Mx}$, as well as for $CarH_{Tt}$ (compare Figure 4A with 4D). Furthermore, in *M. xanthus* MR2648 with enhanced intracellular AdoRhbl, $CarH_{Mx}$ or $CarH_{Tt}$ repressor activity was now observed in the dark, and this was not relieved by light (yellow colony colour under both conditions; compare Figure 4E with 4B). Thus, at adequate cellular levels, AdoRhbl blocks photoregulation, while imitating AdoCbl in driving CarH self-interaction and repression of carotenoid synthesis in the dark.

To gain further structural insights, we performed in silico modelling together with classical molecular dynamics (MD) calculations for the AdoRhbl-$CarH_{Tt}$-DNA complex based on the crystal structure with the AdoCbl ligand[8] (Figure 5), and then compared them with equivalent simulations for AdoCbl.[10j] We also performed QM/MM–MD calculations for AdoRhbl in the $CarH_{Tt}$-DNA complex at the level of DFT (density functional theory) to validate the classical simulations.

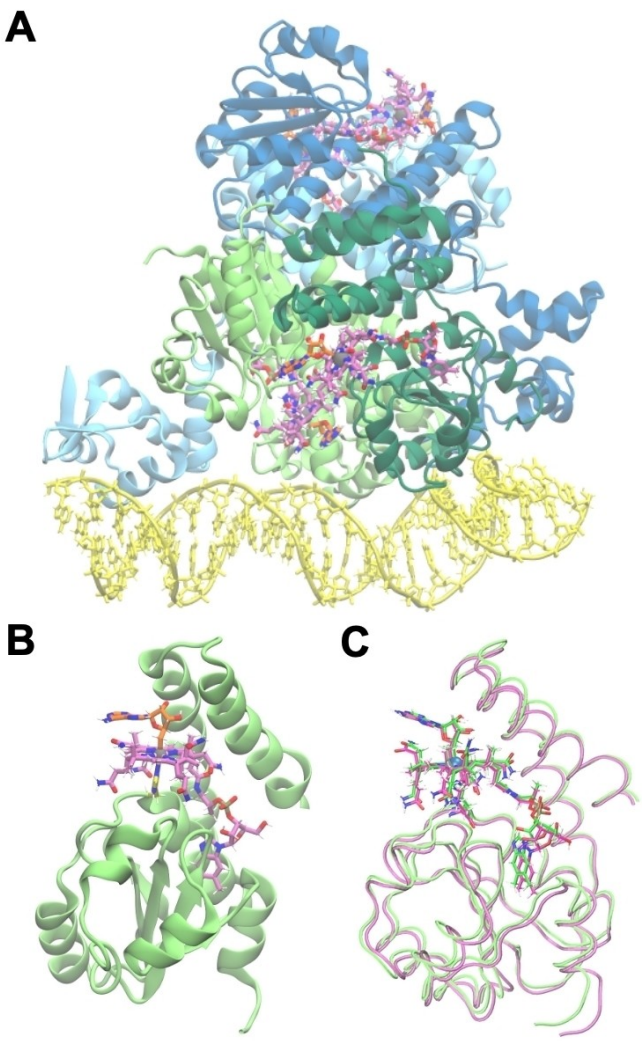

Figure 5. Model of the calculated AdoRhbl-$CarH_{Tt}$-DNA complex. **(A)** The AdoRhbl-$CarH_{Tt}$-DNA model starting from the AdoCbl-$CarH_{Tt}$-DNA crystal structure (PDB ID: 5C8E). Each protomer (light/dark blue and light/dark green ribbon representation) is bound to one AdoRhbl molecule in liquorice representation with C atoms in magenta (corrin ring), yellow (lower axial H177), and orange (Ado), with Rh^{III} as grey sphere and DNA double-helix in yellow. **(B)** The simulated AdoRhbl-$CarH_{Tt}$-DNA system protomer B_{12}-binding domain with bound AdoRhbl. **(C)** Superposition of representative average MD B_{12}-binding domain protomer structures in the AdoCbl-$CarH_{Tt}$ and AdoRhbl-$CarH_{Tt}$ DNA complexes (protein backbone in lime-green and magenta, respectively). In liquorice representation are bound AdoCbl (carbon skeleton, lime-green, Co, blue sphere) and bound AdoRhbl (carbon skeleton, magenta; Rh, gray sphere).

First, we analyzed metal coordination spheres in AdoCbl and AdoRhbl in the $CarH_{Tt}$-DNA complex, finding a well-defined Rh^{III} coordination sphere in AdoRhbl-$CarH_{Tt}$. QM calculations indicate that, compared to Co^{III}, the Rh^{III}-center displays about 0.1 Å longer bonds with Ado-C5′ and the four corrin ring nitrogens, qualitatively consistent with the crystal structures of the two cofactors,[12a] while the bond-

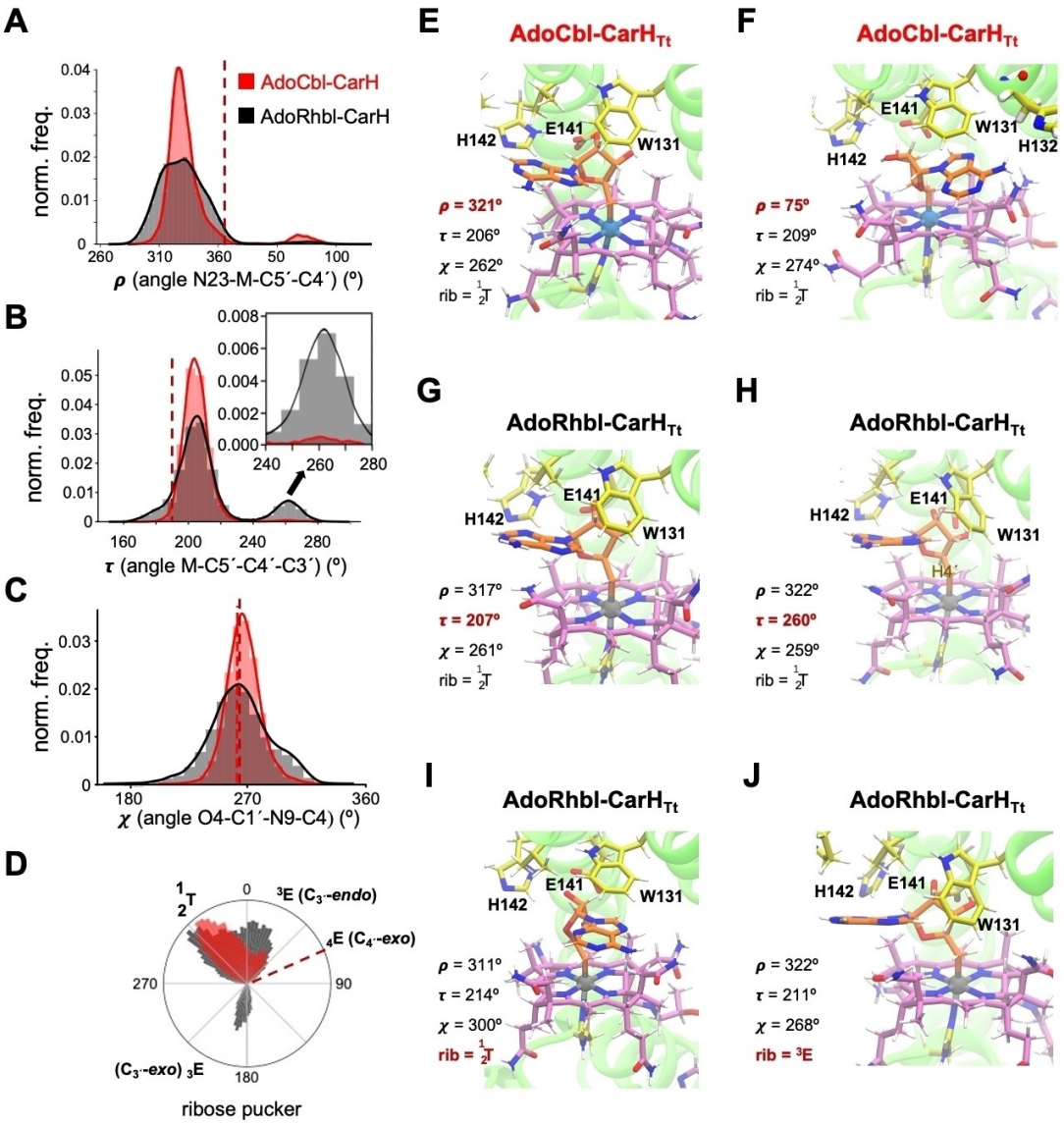

Figure 6. AdoRhbl mimics AdoCbl in binding to CarH but displays a broader conformational landscape in classic MD simulations. Left: Panels indicating relative populations of the four main conformational parameters of the Ado moiety in CarH$_{Tt}$-bound AdoCbl (red traces) and AdoRhbl (black traces). (**A**) Torsion angle ρ describing the orientation of the C4′–C5′ bond of the Ado ligand with respect to the corrin core. (**B**) Torsion angle τ describing orientation of the Ado ribose unit around the C4–C5′ bond (note that at $\tau = 240°$ HC4′ and the central metal are *syn*-planar; see also Figure S13). Inset: Magnified τ distribution around 260°. (**C**) Dihedral torsion angle χ describing relative orientations of the adenine versus ribose units.[27] (**D**) Polar plot for ribose sugar pucker pseudo-dihedral angle[27] distributions (scaled to the same maximum y-value to highlight differences in populations) for CarH$_{Tt}$-bound AdoCbl (red) and AdoRhbl (grey). Red dashed lines in panels **A**–**D** represent values in the AdoCbl-CarH$_{Tt}$-DNA X-ray structure.[8c] Center and right panels **E**–**J**: Close-ups of the CarH$_{Tt}$ binding site pocket with Ado of bound AdoCbl or AdoRhbl. Protein backbone: lime green; C atoms of binding residues in yellow, of corrin ring in magenta and upper axial Ado in orange; Co(III)-center: blue ball; Rh(III)-center: grey ball. Major calculated structures for CarH$_{Tt}$-bound AdoCbl sampled for $\rho = 321°$ (**E**) and 75° (**F**) and of AdoRhbl sampled near $\rho = 320°$ and $\tau = 207°$ (**G**) or 260° (**H**); with adenine moiety in $^1_2$T ($\chi = 300°$) conformation (**I**), and with ^{3}E Ado ribose pucker (~25°) (**J**). In panels **E**–**J**, values for the four main Ado conformational parameters are indicated.

length to the DMB-nitrogen remained unaltered (see Table S3).

We then performed classic MD simulations gathering 2 μs of cumulative sampling for the AdoRhbl-CarH$_{Tt}$-DNA complex (Figure S8). These did not reveal notable differences in the geometries of the corrin ring and DMB moiety in the AdoRhbl-CarH$_{Tt}$ from the earlier simulated AdoCbl-CarH$_{Tt}$-DNA models.[10j] Classical MD and hybrid QM/MM–MD simulations indicated similar interactions between the protein and AdoCbl or AdoRhbl. However, whereas the main interactions between AdoRhbl and CarH$_{Tt}$ residues in the Ado-binding pocket mirrored those of AdoCbl, most of the residues involved in the AdoRhbl-CarH$_{Tt}$-DNA complex displayed higher RMSD values (Figure S9). Indeed, the occupancies of key CarH$_{Tt}$ residues in the Ado-binding site were, on average, lower for AdoRhbl than for AdoCbl, and

not all interactions observed with AdoRhbl were present with AdoCbl (Figure 6 and Figure S10, Tables S4 to S7).

Clearly, $CarH_{Tt}$ does not adapt to AdoRhbl as well as to its natural cofactor AdoCbl in its electronic ground state. However, in the dominant conformers of both the calculated AdoRhbl-$CarH_{Tt}$-DNA and AdoCbl-$CarH_{Tt}$-DNA complexes, the Ado group is similarly reoriented (ρ ca. 320°). The calculations also suggest that AdoRhbl explores a broader conformational landscape (Figure 6). Interestingly, in the $CarH_{Tt}$-DNA complex, Ado undergoes more extensive reorientation around the C5′–C4′-bond in AdoRhbl than in AdoCbl. Furthermore, while the dominant ribose puckering in AdoCbl-$CarH_{Tt}$-DNA crystal structure[8] is close to ^{3}E observed in unbound AdoCbl,[1] MD and QM/MM–MD calculations (Figures S10 to S12) suggest a $^{1}_{2}$T-twist in the AdoCbl-CarH complex, and a minor structure with ^{3}E puckering (Figures 6 and S11). These structures enable H-bonding with the ribose 2′ and 3′-OH groups, while also preserving strong stacking interactions. In the AdoRhbl-$CarH_{Tt}$-DNA complex, the ribose is again primarily in the $^{1}_{2}$T-twist and ^{3}E conformations but it also samples $_{3}$E. The Chi (χ) dihedral torsion angle between the Ado-group ribose and adenine moieties also suggests broader conformational range for AdoRhbl in $CarH_{Tt}$, compared to a more narrowly confined distribution for AdoCbl in $CarH_{Tt}$ (Figure 6C).

The well-structured ligand-binding site in $CarH_{Tt,}$ provides a precise fit for AdoCbl binding in its ground state. This is crucial for the proper control of the photochemical reaction and its dynamics.[10a,f,g] Note that in the AdoCbl-dependent radical enzymes, the substrate-loaded protein not only strains the Ado group, activating AdoCbl for Co–C bond homolysis, but also strictly controls the reaction trajectories,[2,22] for which specific Ado-group conformational adaptations are considered relevant.[2a,23] We suggest that perturbations in the intrinsic dynamics of $CarH_{Tt}$ from the binding of AdoRhbl, a 'dummy' ligand for AdoCbl with a roughly 0.1 Å longer metal-C bond, help explore the Ado-binding site when harboring photoexcited AdoCbl, which was deduced to display a slightly elongated metal-C bond.[10f] A proposed mechanism for the unique CarH photocleavage of AdoCbl is H-transfer from C4′ accompanying Co–C bond cleavage yielding a presumably six-coordinate cob(III)alamin hydride (equivalent, formally, to a Co-protonated cob(I)alamin),[10d,11] which also behaves as a very acidic Co-protonated cob(I)alamin.[24] In fact, the formation of a Co^{I}-corrin species in the photoexcited AdoCbl-$CarH_{Tt}$ complex within milliseconds was very recently reported.[10a] Hence, the positioning of HC4' relative to the cobalt ion in (photoexcited) CarH-bound AdoCbl would be critical.[10d,f,g] Our calculated structural insights concerning the position and distance of HC4′ with respect to the metal centers in the CarH-bound corrins are, therefore, particularly relevant (Figures 6 and S13). The calculated structures specifically suggest the feasibility of a 60° rotation around the C5′–C4′ bond of the Ado group (Figure 6B) that would move HC4′ from one *syn*-clinal position relative to the metal to another one only about 20° beyond the *syn*-planar arrangement. Such a range of transient conformations would be suited for a concerted *syn*-1,2-elimination[25] across the Ado C5′–C4′ bond of AdoCbl to generate the observed nonreactive 4′,5′-anhydroadenosine AdoCbl-CarH photochemical product[10d] in a single elimination step.

Conclusion

The amazing photoregulatory activity of CarH photoreceptors relies on their AdoCbl ligand to photomodulate tetramerization and sequence specific DNA binding, combined with specific light-induced decomposition of the bound AdoCbl, activating gene expression.[5b–d] Here, the antivitamin B_{12} AdoRhbl[12a] was examined for its possible role as an unprecedented anti-photoregulatory ligand. The work reported here shows that AdoRhbl inhibits CarH photoregulatory function and that its uptake into bacterial cells mediated by the B_{12} transporter proteins BtuBCDF is comparable to that of AdoCbl. In fact, AdoRhbl acts as a highly effective anti-photoregulatory ligand that inhibits photoreceptor function by imitating the specific mode of AdoCbl binding to the CarH photoreceptor to drive tetramerization and DNA binding. Yet, AdoRhbl remains photostable, despite the basic structural changes that it undergoes upon binding to CarH. However, AdoRhbl is required at higher concentrations than AdoCbl in representative bacteria for CarH oligomerization and repressor activity in vivo. This is consistent with the ~25-fold lower in vitro affinity of AdoRhbl for CarH. The lower affinity of AdoRhbl may be due to the substantial coordinative restructuring required for base-off/His-on binding as well as to the more extensive conformational sampling of the Ado moiety in AdoRhbl than in AdoCbl, as deduced from the computational analysis.

Despite the availability of detailed crystallographic structures of dark-state CarH, free and in complex with DNA, and its light-exposed form,[5b,8,10a] the reactivity of its photoexcited state has remained an obstinate puzzle.[5d,10a,d–f,n] CarH binding strongly extends the light-excited state lifetime of AdoCbl,[10f] and also ensures the quantitative Co–C bond cleavage in a remarkable formal photoelimination reaction.[5b,10d] Interestingly, a Co(II)corrin intermediate is not detected, the characteristic direct product from photoinduced homolysis of the AdoCbl Co–C bond in solution,[4c] and in the AdoCbl-dependent radical enzyme glutamate mutase.[26] This suggests a precise structural reorganization of the photoexcited AdoCbl-$CarH_{Tt}$ complex in the active site of CarH.[10e–g] Clearly, the active site is instrumental in constraining the hypothetical Co–C bond cleavage of the remarkably long-lived photoexcited AdoCbl trajectory to the formal elimination reaction.

Consistent with the experimental data for AdoRhbl reported here, MD simulations based on the AdoCbl-$CarH_{Tt}$-DNA crystal structure suggest that in the interactions with CarH, AdoRhbl largely imitates the restructuring observed with the natural analogue AdoCbl, which binds base-off/His-on with its 'upper' Ado-ligand reoriented via rotation around its organometallic bond (Figure 6).[8,11] In the predominant structures, key residues of the CarH-

AdoRhbl interface are presented in orientations closely matching those for CarH-AdoCbl.[8] Furthermore, our calculated structures suggest a specifically limited complementary plasticity of the protein interface, providing key binding interactions to the Ado group of AdoCbl or of AdoRhbl. A significant conformational flexibility of the ribose moiety is a key factor enabling the critical reorientation of the Ado group. However, Ado and active site residues in CarH-bound AdoRhbl explore a wider conformational space than with AdoCbl (Figures 6 and S8 to S13).

Replacing the AdoCbl ligand in the CarH-complex by its light stable Rh-analogue AdoRhbl, with a 0.1 Å longer metal-C bond, may thus help explore the capacity of CarH to accommodate relevant transient photoexcited state(s) of bound AdoCbl, deduced to display a minor elongation of the Co–C bond.[10f] Enhanced modes of conformational restructuring from replacing AdoCbl in $CarH_{Tt}$ by AdoRhbl are revealed in the calculations, providing structural models for the hypothetical transient excited state structures of the AdoCbl-CarH complex crucial for the intricate control of the non-radical photocleavage by its active site. The deduced dynamics support the feasibility of a rotation around the Ado C5′–C4′ bond in the photoexcited AdoCbl-$CarH_{Tt}$-DNA complex, a critical motion for the hypothetical CarH-orchestrated photoinduced *syn*-1,2-elimination, as a non-radical mechanism to the observed intermediate Co^{I}-corrin and to 4′,5′- anhydroadenosine.[10a,d] Clearly, CarH may have evolved not merely to bind the natural AdoCbl cofactor but also to guide the trajectory of its transient light-activated states via a specific selective binding complement along the crucial path to stable photoproducts.

In conclusion, our research characterizes AdoRhbl, an engineered antivitamin B_{12}, as an unprecedented and highly efficient anti-photoregulatory ligand.[12a,14c,15d] Serving as a stable structural AdoCbl mimic, even in the presence of CarH, AdoRhbl proves to be a potent inhibitor not only for prevalent bacterial photoreceptors, but also potentially for numerous AdoCbl-dependent photoresponsive proteins of unknown function, identified through genome data.[5b–d,6–7] This positions AdoRhbl within a new category of selective and broadly effective potential antibiotics. Furthermore, our computational analysis provides a structural model of the AdoRhbl-CarH-DNA complex. According to this model, the photoexcited CarH-bound AdoCbl can dynamically adopt structures compatible with a specific *syn*-1,2-elimination mechanism for the proposed concerted photochemical decomposition of the AdoCbl-CarH complex,[10n] averting radical products.

Acknowledgements

We thank Prof. S.J. Booker and Hayley Knox (Penn State University, USA) for plasmid pBAD42-*btuCEDFB* and related protocols. This work was funded by MCIN/AEI/10.13039/501100011033 and "ERDF A way of making Europe", grants PGC2018-094635-B-C21 and PID2021-123336NB-C21 to M.E.-A. and Ph.D. fellowship to R.P.-C.; PGC2018-094635-B-C22 and PID2021-123336NB-C22 to S.P; PID2021-122478NB-100 to M.O.; Juan de la Cierva investigator grant to J.A; Severo Ochoa Institutional Award to IRB-Barcelona; Fundación Séneca-Spain grants 20992/PI/18 and 21939/PI/22 to M.E.-A.; Catalan SGR, European Union BioExcel-3 project 1010932290 (European Union's Horizon 2020 research and innovation program), Instituto Nacional de Bioinformática, Biomolecular and Bioinformatics Resources Platform (ISCIII PT 13/0001/0030) to MO; Austrian Science Fund (projects P-28892 and P-33059) to BK; and the Biotechnology and Biological Sciences Research Council (BBSRC), project grant BB/X001946/1, and BBSRC Institute Strategic Programme Food Innovation and Health BB/R012512/1, project BBS/E/F/000PR10346 to MJW.

Conflict of Interest

The authors declare no conflict of interest.

Data Availability Statement

The data that support the findings of this study are available in the supplementary material of this article.f

Keywords: antivitamin B_{12} · photoreceptor · cobalamin · photoinhibitor · rhodium

[1] a) P. G. Lenhert, D. C. Hodgkin, *Nature* **1961**, *192*, 937–938; b) A. Eschenmoser, *Angew. Chem. Int. Ed.* **1988**, *27*, 5–39; c) K. Gruber, B. Puffer, B. Kräutler, *Chem. Soc. Rev.* **2011**, *40*, 4346–4363.

[2] a) R. Banerjee, S. W. Ragsdale, *Annu. Rev. Biochem.* **2003**, *72*, 209–247; b) J. Bridwell-Rabb, C. L. Drennan, *Curr. Opin. Chem. Biol.* **2017**, *37*, 63–70; c) M. Giedyk, K. Goliszewska, D. Gryko, *Chem. Soc. Rev.* **2015**, *44*, 3391–3404; d) B. Kräutler, B. Puffer, in *Handbook of Porphyrin Science, Vol. 25* (Ed.: K. M. Kadish, K. M. Smith, R. Guilard), World Scientific **2012**, pp. 131–263.

[3] J. Halpern, *Science* **1985**, *227*, 869–875.

[4] a) H. Weissbach, J. Toohey, H. A. Barker, *Proc. Natl. Acad. Sci. USA* **1959**, *45*, 521–525; b) A. S. Rury, T. E. Wiley, R. J. Sension, *Acc. Chem. Res.* **2015**, *48*, 860–867; c) J. F. Endicott, T. L. Netzel, *J. Am. Chem. Soc.* **1979**, *101*, 4000–4002.

[5] a) J. M. Ortiz-Guerrero, M. C. Polanco, F. J. Murillo, S. Padmanabhan, M. Elias-Arnanz, *Proc. Natl. Acad. Sci. USA* **2011**, *108*, 7565–7570; b) S. Padmanabhan, M. Jost, C. L. Drennan, M. Elías-Arnanz, *Annu. Rev. Biochem.* **2017**, *86*, 485–514; c) S. Padmanabhan, R. Pérez-Castaño, M. Elías-Arnanz, *Curr. Opin. Struct. Biol.* **2019**, *57*, 47–55; d) S. Padmanabhan, R. Pérez-Castaño, L. Osete-Alcaraz, M. C. Polanco, M. Elías-Arnanz, *Vitam. Horm.* **2022**, *119*, 149–184.

[6] a) Z. Cheng, K. Li, L. A. Hammad, J. A. Karty, C. E. Bauer, *Mol. Microbiol.* **2014**, *91*, 649–664; b) Z. Cheng, H. Yamamoto, C. E. Bauer, *Trends Biochem. Sci.* **2016**, *41*, 647–650; c) H. Yamamoto, M. Fang, V. Dragnea, C. E. Bauer, *eLife* **2018**, *7*, e39028.

[7] T. Schneider, Y. Tan, H. Li, J. S. Fisher, D. Zhang, *Comput. Struct. Biotechnol. J.* **2022**, *20*, 261–273.

[8] M. Jost, J. Fernandez-Zapata, M. C. Polanco, J. M. Ortiz-Guerrero, P. Y. Chen, G. Kang, S. Padmanabhan, M. Elias-Arnanz, C. L. Drennan, *Nature* **2015**, *526*, 536–541.

[9] a) S. Kainrath, M. Stadler, E. Reichhart, M. Distel, H. Janovjak, *Angew. Chem.* **2017**, *56*, 4608–4611; b) R. Wang, Z. Yang, J. Luo, I. M. Hsing, F. Sun, *Proc. Natl. Acad. Sci. USA* **2017**, *114*, 5912–5917; c) C. Chatelle, R. Ochoa-Fernandez, R. Engesser, N. Schneider, H. M. Beyer, A. R. Jones, J. Timmer, M. D. Zurbriggen, W. Weber, *ACS Synth. Biol.* **2018**, *7*, 1349–1358; d) D. Xu, J. Ricken, S. Wegner, *Chem. Eur. J.* **2020**; e) O. P. Narayan, X. Mu, O. Hasturk, D. L. Kaplan, *Acta Biomater.* **2021**, *121*, 214–223; f) M. Mansouri, M.-D. Hussherr, T. Strittmatter, P. Buchmann, S. Xue, G. Camenisch, M. Fussenegger, *Nat. Commun.* **2021**, *12*, 3388; g) X. Yang, B. H. R. Gerroll, Y. Jiang, A. Kumar, Y. S. Zubi, L. A. Baker, J. C. Lewis, *ACS Catal.* **2022**, *12*, 935–942; h) Z. Yang, H. K. F. Fok, J. Luo, Y. Yang, R. Wang, X. Huang, F. Sun, *Sci. Adv.* **2022**, *8*, eabm5482; i) J. Li, A. Kumar, J. C. Lewis, *Angew. Chem. Int. Ed. Engl.* **2023**, e202312893.

[10] a) H. Poddar, R. Rios-Santacruz, D. J. Heyes, M. Shanmugam, A. Brookfield, L. O. Johannissen, C. W. Levy, L. N. Jeffreys, S. Zhang, M. Sakuma, J. P. Colletier, S. Hay, G. Schirò, M. Weik, N. S. Scrutton, D. Leys, *Nat. Commun.* **2023**, *14*, 5082; b) M. C. Pérez-Marín, S. Padmanabhan, M. C. Polanco, F. J. Murillo, M. Elías-Arnanz, *Mol. Microbiol.* **2008**, *67*, 804–819; c) A. I. Díez, J. M. Ortiz-Guerrero, A. Ortega, M. Elías-Arnanz, S. Padmanabhan, J. García de la Torre, *Eur. Biophys. J.* **2013**, *42*, 463–476; d) M. Jost, J. H. Simpson, C. L. Drennan, *Biochemistry* **2015**, *54*, 3231–3234; e) R. J. Kutta, S. J. Hardman, L. O. Johannissen, B. Bellina, H. L. Messiha, J. M. Ortiz-Guerrero, M. Elías-Arnanz, S. Padmanabhan, P. Barran, N. S. Scrutton, A. R. Jones, *Nat. Commun.* **2015**, *6*, 7907; f) N. A. Miller, A. K. Kaneshiro, A. Konar, R. Alonso-Mori, A. Britz, A. Deb, J. M. Glownia, J. D. Koralek, L. Mallik, J. H. Meadows, L. B. Michocki, T. B. van Driel, M. Koutmos, S. Padmanabhan, M. Elías-Arnanz, K. J. Kubarych, E. N. G. Marsh, J. E. Penner-Hahn, R. J. Sension, *J. Phys. Chem. B* **2020**, *124*, 10732–10738; g) M. J. Toda, A. A. Mamun, P. Lodowski, P. M. Kozlowski, *J. Photochem. Photobiol. B* **2020**, *209*, 111919; h) I. S. Camacho, R. Black, D. J. Heyes, L. O. Johannissen, L. A. I. Ramakers, B. Bellina, P. E. Barran, S. Hay, A. R. Jones, *Chem. Sci.* **2021**, *12*, 8333–8341; i) H. Takano, K. Mise, K. Hagiwara, N. Hirata, S. Watanabe, M. Toriyabe, H. Shiratori-Takano, K. Ueda, *J. Bacteriol.* **2015**, *197*, 2301–2315; j) J. Fernández-Zapata, R. Pérez-Castaño, J. Aranda, F. Colizzi, M. C. Polanco, M. Orozco, S. Padmanabhan, M. Elías-Arnanz, *J. Biol. Chem.* **2018**, *293*, 17888–17905; k) C. L. Cooper, N. Panitz, T. A. Edwards, P. Goyal, *Biophys. J.* **2021**, *120*, 3688–3696; l) R. Pérez-Castaño, E. Bastida-Martínez, J. Fernández Zapata, M. D. C. Polanco, M. L. Galbis-Martínez, A. A. Iniesta, M. Fontes, S. Padmanabhan, M. Elías-Arnanz, *Environ. Microbiol.* **2022**; m) M. J. Mackintosh, P. Lodowski, P. M. Kozlowski, *J. Photochem. Photobiol. B* **2023**, 112751; n) I. S. Camacho, E. Wall, I. V. Sazanovich, E. Gozzard, M. Towrie, N. T. Hunt, S. Hay, A. R. Jones, *Chem. Commun. (Camb.)* **2023**, *59*, 13014–13017.

[11] K. Gruber, B. Kräutler, *Angew. Chem. Int. Ed. Engl.* **2016**, *55*, 5638–5640.

[12] a) F. J. Widner, A. D. Lawrence, E. Deery, D. Heldt, S. Frank, K. Gruber, K. Wurst, M. J. Warren, B. Kräutler, *Angew. Chem. Int. Ed.* **2016**, *55*, 11281–11286; b) F. J. Widner, C. Kieninger, K. Wurst, E. Deery, M. J. Warren, B. Kräutler, *Synthesis* **2021**, *53*, 332–337; c) V. B. Koppenhagen, in *B_{12}, Vol. 2* (Ed.: D. Dolphin), John Wiley & Sons **1982**, pp. 105–150.

[13] a) A. Eschenmoser, *Angew. Chem. Int. Ed.* **2011**, *50*, 12412–12472; b) D. Osman, A. Cooke, T. R. Young, E. Deery, N. J. Robinson, M. J. Warren, *Biochim. Biophys. Acta Mol. Cell Res.* **2021**, *1868*, 118896; c) F. Zelder, *Chem. Commun. (Camb.)* **2015**, *51*, 14004–14017; d) J. M. Pratt, in *Chemistry and Biochemistry of B_{12}* (Ed.: R. Banerjee), John Wiley & Sons, Inc. **1999**, pp. 73–112.

[14] a) C. Kieninger, J. A. Baker, M. Podewitz, K. Wurst, S. Jockusch, A. D. Lawrence, E. Deery, K. Gruber, K. R. Liedl, M. J. Warren, B. Kräutler, *Angew. Chem. Int. Ed.* **2019**, *58*, 14568–14572; b) C. Kieninger, K. Wurst, M. Podewitz, M. Stanley, E. Deery, A. D. Lawrence, K. R. Liedl, M. J. Warren, B. Kräutler, *Angew. Chem. Int. Ed.* **2020**, *59*, 20129-20136 ; c) B. Kräutler, *Chem. Eur. J.* **2020**, *26*, 15438–15445; d) M. Wiedemair, C. Kieninger, K. Wurst, M. Podewitz, E. Deery, M. D. Paxhia, M. J. Warren, B. Kräutler, *Helv. Chim. Acta* **2023**, *106*, e202200158.

[15] a) E. Mutti, M. Ruetz, H. Birn, B. Kräutler, E. Nexo, *PLoS One* **2013**, *8*, e75312; b) B. Kräutler, *Chem. Eur. J.* **2015**, *21*, 11280–11287; c) M. B. Guzzo, H. T. Nguyen, T. H. Pham, M. Wyszczelska-Rokiel, H. Jakubowski, K. A. Wolff, S. Ogwang, J. L. Timpona, S. Gogula, M. R. Jacobs, M. Ruetz, B. Kräutler, D. W. Jacobsen, G. F. Zhang, L. Nguyen, *PLoS Pathog.* **2016**, *12*, e1005949; d) B. Kräutler, *Vitam. Horm.* **2022**, *119*, 221–240.

[16] T. Toraya, *Arch. Biochem. Biophys.* **2014**, *544*, 40–57.

[17] a) J. M. Pratt, *Inorganic Chemistry of Vitamin B_{12}*, Academic Press Inc. **1972**; b) T. C. Brunold, K. S. Conrad, M. D. Liptak, K. Park, *Coord. Chem. Rev.* **2009**, *253*, 779–794.

[18] M. P. Jensen, J. Halpern, *J. Am. Chem. Soc.* **1999**, *121*, 2181–2192.

[19] N. D. Lanz, A. J. Blaszczyk, E. L. McCarthy, B. Wang, R. X. Wang, B. S. Jones, S. J. Booker, *Biochemistry* **2018**, *57*, 1475–1490.

[20] a) J. R. Roth, J. G. Lawrence, T. A. Bobik, *Annu. Rev. Microbiol.* **1996**, *50*, 137–181; b) A. Nahvi, J. E. Barrick, R. R. Breaker, *Nucleic Acids Res.* **2004**, *32*, 143–150.

[21] a) L. Randaccio, S. Geremia, N. Demitri, J. Wuerges, *Molecules* **2010**, *15*, 3228–3259; b) M. Nijland, J. M. Martínez Felices, D. J. Slotboom, C. Thangaratnarajah, *Vitam. Horm.* **2022**, *119*, 121–148.

[22] a) J. Rétey, *Angew. Chem. Int. Ed.* **1990**, *29*, 355–361; b) K. Gruber, V. Csitkovits, A. Łyskowski, C. Kratky, B. Kräutler, *Angew. Chem. Int. Ed.* **2022**, *61*, e202208295.

[23] a) K. Gruber, R. Reitzer, C. Kratky, *Angew. Chem. Int. Ed.* **2001**, *40*, 3377–3380; b) T. Toraya, *Chem. Rev.* **2003**, *103*, 2095–2128.

[24] a) D. Lexa, J. M. Saveant, *J. Am. Chem. Soc.* **1976**, *98*, 2652–2658; b) S. M. Chemaly, J. M. Pratt, *J. Chem. Soc. Dalton Trans.* **1984**, 595–599.

[25] J. H. Grate, G. N. Schrauzer, *J. Am. Chem. Soc.* **1979**, *101*, 4601–4611.

[26] a) R. J. Sension, A. G. Cole, A. D. Harris, C. C. Fox, N. W. Woodbury, S. Lin, E. N. Marsh, *J. Am. Chem. Soc.* **2004**, *126*, 1598–1599; b) K. Gruber, C. Kratky, *Curr. Opin. Chem. Biol.* **2002**, *6*, 598–603.

[27] W. Sanger, in *Principles of Nucleic Acid Structure*, 1 ed., Springer New York, NY, New York, NY **1984**, pp. 51–104.

Manuscript received: January 23, 2024
Accepted manuscript online: February 28, 2024
Version of record online: March 19, 2024